

Unusually large earthquakes inferred from tsunami deposits along the Kuril trench

Futoshi Nanayama¹, Kenji Satake¹, Ryuta Furukawa¹, Koichi Shimokawa¹, Brian F. Atwater², Kiyoyuki Shigeno³ & Shigeru Yamaki⁴

¹Geological Survey of Japan, National Institute of Advanced Industrial Science and Technology, Tsukuba 305-8567, Japan

²US Geological Survey at University of Washington, Seattle, Washington 98195-1310, USA

³Meiji Consultant Co. Ltd, Chuo-ku, Sapporo 064-0807, Japan

⁴Seamus Ltd, Toyosaka, Niigata 950-3304, Japan

The Pacific plate converges with northeastern Eurasia at a rate of 8–9 m per century along the Kamchatka, Kuril and Japan trenches¹. Along the southern Kuril trench, which faces the Japanese island of Hokkaido, this fast subduction has recurrently generated earthquakes with magnitudes of up to ~8 over the past two centuries^{2–6}. These historical events, on rupture segments 100–200 km long, have been considered characteristic of Hokkaido's plate-boundary earthquakes^{7,8}. But here we use deposits of prehistoric tsunamis to infer the infrequent occurrence of larger earthquakes generated from longer ruptures. Many of these tsunami deposits form sheets of sand that extend kilometres inland from the deposits of historical tsunamis. Stratigraphic series of extensive sand sheets, intercalated with dated volcanic-ash layers, show that such unusually large tsunamis occurred about every 500 years on average over the past 2,000–7,000 years,

most recently ~350 years ago. Numerical simulations of these tsunamis are best explained by earthquakes that individually rupture multiple segments along the southern Kuril trench. We infer that such multi-segment earthquakes persistently recur among a larger number of single-segment events.

Eastern Hokkaido's largest well-documented interplate earthquake—the Tokachi-oki earthquake of moment magnitude (M_w) 8.1 in 1952 (ref. 4)—shook much of northeast Japan and generated tsunami waves 1–4 m high along the Hokkaido coast⁹. The ensuing 1973 Nemuro-oki earthquake (M_w 7.8)^{2,3}, from a shorter rupture to the east, had similar but more localized effects. Eastern Hokkaido previously suffered great earthquakes in 1843 (tsunami magnitude M_t 8.0) and 1894 (M_t 8.2)^{10,11}. The ruptures in 1843 and 1894 probably resembled those in 1952 and 1973, respectively^{5,6} (Fig. 1). Eastern Hokkaido may also have a late Holocene history of coseismic or postseismic emergence at estuaries¹². The region's most direct and compelling evidence for prehistoric earthquakes, however, consists of sheets of sand near the open coast.

Although tsunamis have left sand sheets on many coasts^{13,14}, few reported examples rival eastern Hokkaido's in landward extent or in number of successive sheets (Fig. 2, Supplementary Information,

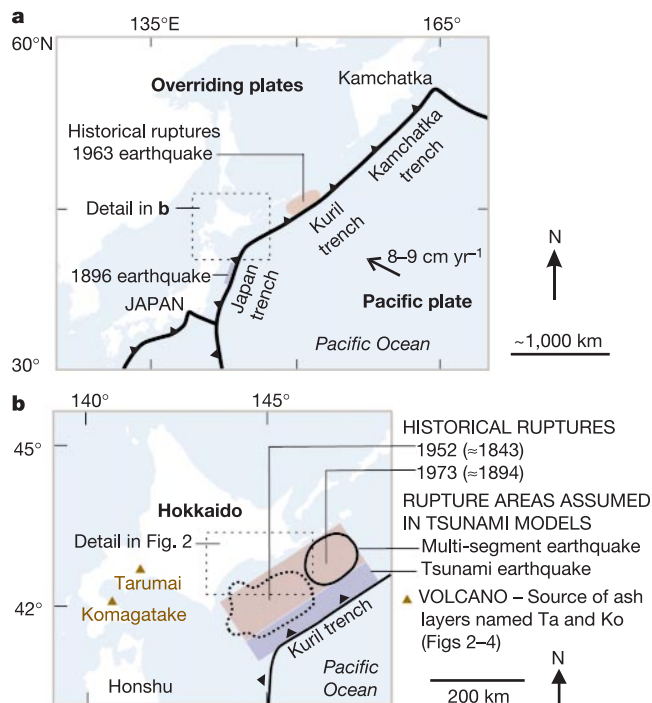


Figure 1 Maps of study area. Barbed lines show seaward edges of subduction zones; teeth point down the plate boundary. **a**, Subduction zone along the Kamchatka, Kuril and Japan trenches, showing rupture areas of 1896 and 1963 earthquakes^{20,23}. **b**, Hokkaido and northernmost Honshu, showing rupture areas of the 1952 and 1973 events^{2,4}, estimated locations of 1843 and 1894 earthquakes (rupture areas poorly known^{5,6}), and rupture areas of hypothetical earthquakes used in tsunami simulations (Fig. 2c).

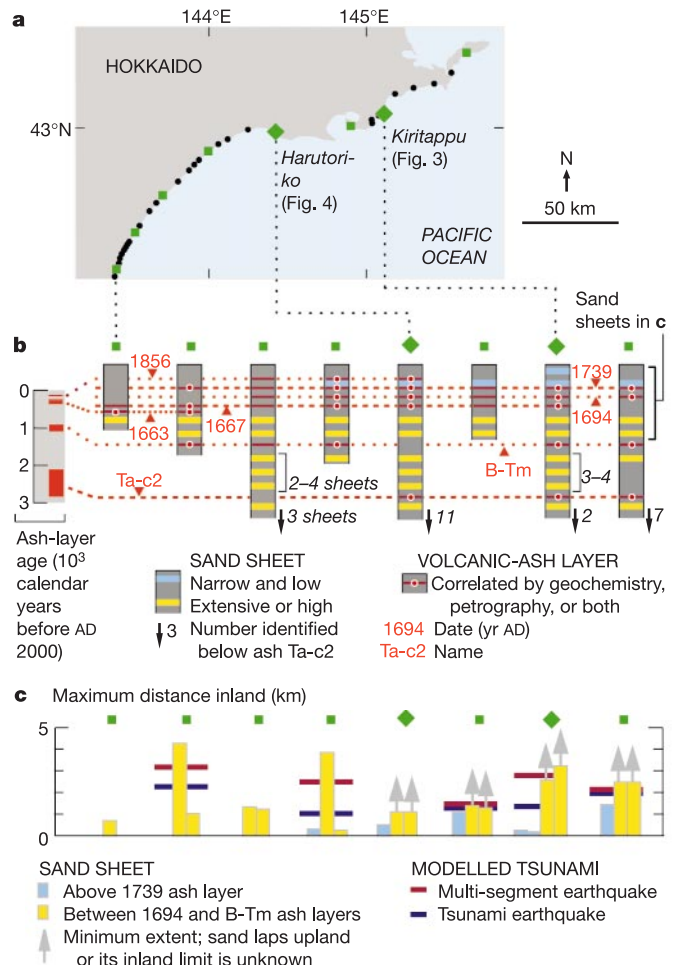


Figure 2 Summary of tsunami deposits in eastern Hokkaido and comparison with modelled inundation. Supporting details in Supplementary Tables S1 and S2, and Supplementary Fig. S1. **a**, Sites where prehistoric tsunami deposits have been found. **b**, Correlation of tsunami deposits by volcanic-ash layers. Samples were identified geochemically as in Supplementary Table S2, except for Usu-b, which was identified by petrography only. B-Tm, volcanic ash from Baitousan volcano, on the China–Korea border. **c**, Inland extent of sand sheets, compared with extent of inundation computed for tsunamis from hypothetical earthquakes in Fig. 1b.

and refs 15, 16). Many of Hokkaido's prehistoric sand sheets penetrate hundreds to thousands of metres inland (Fig. 2c). At all sites, the youngest extensive sheet pre-dates a widespread volcanic ash layer from 1694 (ref. 17) and in the southwest it also pre-dates localized ash layers from the 1660s (Fig. 2b). No tsunami or storm surge since 1694 has produced comparable deposits in the region¹⁸. The following examples show that outsize, prehistoric tsunamis repeatedly overran a beach-ridge plain (at Kiritappu; Fig. 3) and invaded a nearby coastal lake or lagoon (Harutori-ko; Fig. 4) at intervals averaging about 500 yr.

The sand sheets at Kiritappu are interbedded with freshwater peat and volcanic ash (Fig. 3). At least five sheets extend about 3 km across the beach-ridge plain, which averages a few metres above sea level. Marine diatoms abound in the sand but not in the intervening peat (Fig. 3d). Four or five extensive sand sheets overlie the volcanic ash Ta-c2 (2,000–3,000 yr old; Supplementary Table S2), and all the sheets that extend more than 200 m inland underlie the Ko-c2 ash (AD 1694; ref. 17).

The long stratigraphic record at Harutori-ko provides evidence for at least 17 tsunamis in the past 7,000 yr (Fig. 4). This lake or lagoon, which contains anoxic bottom water¹⁹, is flanked by Pleistocene uplands and separated from the sea by a 5-m-high beach berm that the 1952 tsunami did not cross (Fig. 4a, b). Deposits from the past 7,000 yr beneath the floor of Harutori-ko consist of laminated mud that alternates with sandy beds 0.1–1.0 m thick. The laminated mud, undisturbed by bottom-dwelling organisms, implies that a seaside berm has prevented tidal mixing in Harutori-ko through much of the Holocene. A core 1 km from the modern beach contains 17 of the sandy beds (Fig. 4c). Some of these beds grade upward from shell-bearing sand, through mud-clast breccia and laminated silt, into organic mud (Fig. 4d). At least four

of the beds lie between the 2,000- to 3,000-yr-old ash and the AD 1694 ash (Fig. 4c).

Large displacements of the sea floor are required to have generated the outsize waves implied by the eastern Hokkaido's prehistoric tsunami deposits. Because bathymetric mapping and seismic profiling along the Kuril and Japan trenches have yet to reveal enormous submarine landslides, we attempted to simulate the waves as products of tectonic displacement during two kinds of submarine earthquakes. One has a broad, multi-segment rupture 300 km by 100 km at 17–51 km depth, with 5 m slip. This M_w 8.4 earthquake, nearly as large as the nearby 1963 Kuril Islands earthquake²⁰ (Fig. 1a), simulates combined rupture of the Hokkaido segments that ruptured in the 1952 and 1973 earthquakes (Fig. 1b). The other is a tsunami earthquake—an event that produces water waves much larger than expected from seismic waves^{21,22}. We assume 5 m of slip on a narrow rupture 300 km by 50 km that extends to the sea floor directly updip from our multi-segment rupture (Fig. 5a). In size and depth, this hypothetical event resembles the tsunami earthquake along the Japan trench in 1896 (Fig. 1a; ref. 23). The 1896 tsunami reached heights over 10 m in northeast Honshu but less than 1 m in the eastern Hokkaido^{11,23}, and it may have been a repeat of an tsunami that devastated northeast Honshu in 1611 (ref. 11).

Although they predict similar tsunami heights at the coast, the two models differ in pattern of sea-floor displacement and in predicted inland extent of inundation. For the Pacific coast of eastern Hokkaido, both models predict tsunami heights mostly in the range 3–10 m (Supplementary Fig. S1b). However, for earthquakes having the same amount of slip, the sea-floor uplift in the multi-segment model is three times wider and 1 m higher than in the tsunami earthquake model (Fig. 5b). Consequently, only the tsunami waves from the broad, multi-segment rupture run far

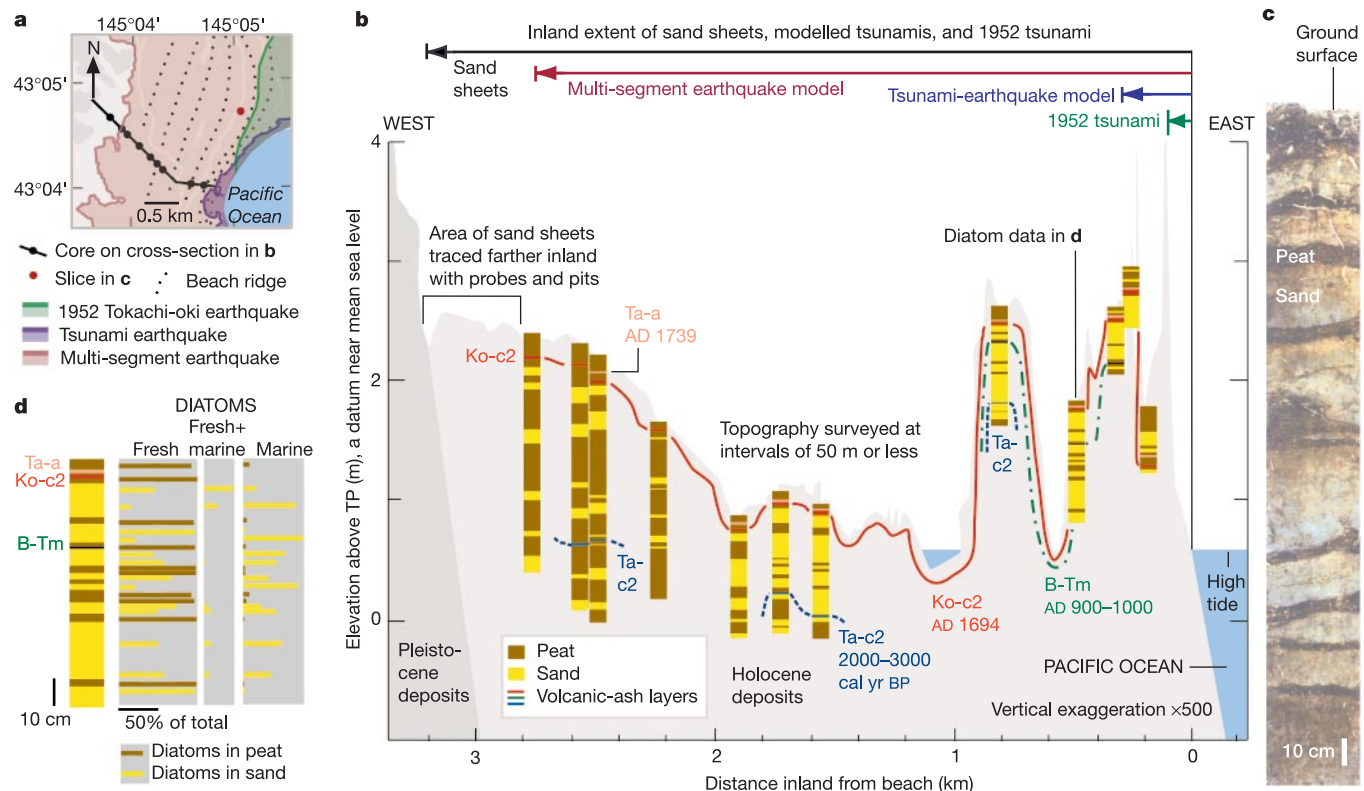


Figure 3 Evidence for outsize tsunamis at Kiritappu. **a**, Index map, showing inundation areas reported for the 1952 tsunami⁹ and computed for the two hypothetical earthquakes in Fig. 1b. **b**, Cross-section of cores correlated by volcanic ash from Tarumai (Ta-a, Ta-c2), Komagatake (Ko-c2) and Baitousan (B-Tm) (ref. 17, Supplementary Table S2). Arrows

at top compare sand-sheet extent with inundation computed from hypothetical earthquakes and with inundation observed for 1952 tsunami⁹. **c**, Sand interbedded with peat in slice collected 0.5 km from the coast (at red dot in **a**). **d**, Diatom assemblages from a core in **b** (supporting details in Supplementary Table S3).

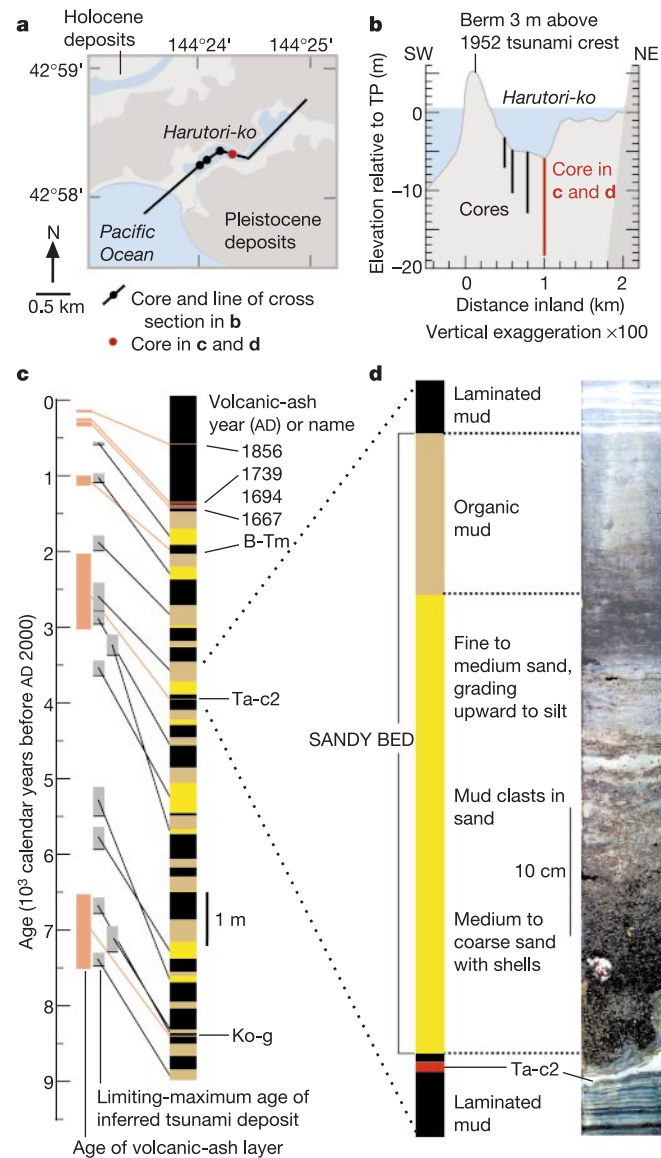


Figure 4 Evidence for outside tsunamis at Harutori-ko. **a, b**, Geomorphic setting. **c**, Generalized stratigraphy from the past 7,000 yr. **d**, Typical sandy bed.

enough inland to approach the sand-sheet limits (Figs 2c and 3a, b). Compared with inundation from the narrow tsunami-earthquake rupture, these waves penetrate farther because their wavelength is broader.

Tsunami deposits from recent millennia in eastern Hokkaido thus imply larger earthquakes and longer recurrence intervals than do records from the region's two historical centuries. The contrasting earthquakes are probably analogous to the successive twentieth-century ruptures that differed in length by factors of two or more at other subduction zones^{24–26}. Similarly, along the Nankai trough of southwest Japan, a multi-segment rupture 500 km long in 1707 broke again, in shorter pieces, as a pair of lesser earthquakes in 1854 and another pair in 1944–46 (ref. 26). Eastern Hokkaido's combination of prehistoric and historical evidence goes beyond these historical examples by implying persistent recurrence of multi-segment earthquakes at a subduction zone that is also subject to single-segment events. This persistence, in turn, implies that variation in rupture mode is characteristic of subduction along the southern Kuril trench. □

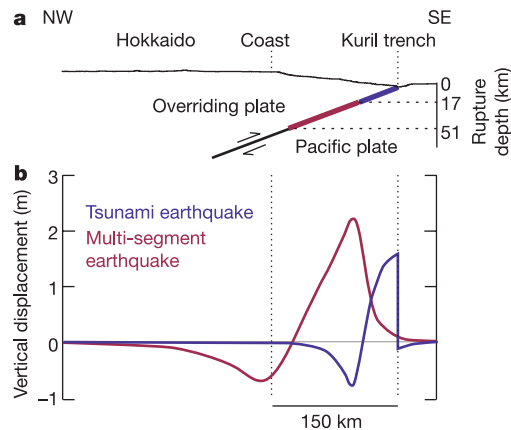


Figure 5 Cross-sectional view of **a**, two fault models and **b**, the sea-floor displacement computed from them.

Methods

In numerical simulations of tsunami inundation, we first computed sea-floor displacement from fault parameters (Fig. 5)²⁷, then used a finite-difference method to solve the nonlinear long-wave equation and the equation of continuity^{28,29}. The minimum grid interval is 225 m along the entire coast in Fig. 2a. To compute inland penetration at Kiritappu (Fig. 3a,b) and other sites in Fig. 2c, we used 25-m grids for bathymetry and topography, and we assumed the moving-boundary condition³⁰. In addition to the two tsunami sources described in the text, we also considered a tsunami earthquake with 10 m of slip (about twice that inferred for the 1896 Sanriku tsunami earthquake), which produces larger coastal heights than shown in Supplementary Fig. S2b but little more inundation distance than shown in Fig. 2c.

Received 20 January; accepted 24 June 2003; doi:10.1038/nature01864.

- DeMets, C. Oblique convergence and deformation along the Kuril and Japan Trenches. *J. Geophys. Res.* **97**, 17615–17625 (1992).
- Aida, I. Reliability of a tsunami source model derived from fault parameters. *J. Phys. Earth* **26**, 57–73 (1978).
- Shimazaki, K. Nemuro-oki earthquake of June 17, 1973: A lithospheric rebound at the upper half of the interface. *Phys. Earth Planet. Inter.* **9**, 314–327 (1974).
- Hirata, K., Geist, E. L., Satake, K., Tanioka, Y. & Yamaki, S. Slip distribution of the 1952 Tokachi-Oki earthquake (M 8.1) along the Kuril trench deduced from tsunami waveform inversion. *J. Geophys. Res.* **108**, 101029/2002JB001976 (2003).
- Hatori, T. Source area of the tsunami off the Nemuro Peninsula in 1973 and its comparison with the tsunami in 1894 [in Japanese with English abstract]. *Spec. Bull. Earthq. Res. Inst. Univ. Tokyo* **13**, 67–76 (1974).
- Hatori, T. Source area of the East Hokkaido Tsunami generated in April, 1843 [in Japanese with English abstract]. *Bull. Earthq. Res. Inst. Univ. Tokyo* **59**, 423–431 (1984).
- Fukao, Y. & Furumoto, M. Stress drops, wave spectra and recurrence intervals of great earthquakes — implications of the Etorofu earthquake of 1958 November 6. *Geophys. J. R. Astron. Soc.* **57**, 23–40 (1979).
- Nishenko, S. P. Circum-Pacific seismic potential: 1989–1999. *Pure Appl. Geophys.* **135**, 169–259 (1991).
- Central Meteorological Observatory The Tokachi earthquake of March 4, 1952 [in Japanese with English abstract]. *Q. J. Seismol.* **17**, 1–135 (1953).
- Abe, K. Quantification of historical tsunamis by the M_1 scale [in Japanese with English abstract]. *Zisin* **52**, 369–377 (1999).
- Watanabe, H. *Comprehensive List of Tsunamis to Hit the Japanese Islands* [in Japanese] (Univ. Tokyo Press, Tokyo, 1998).
- Sawai, Y., Nasu, H. & Yasuda, Y. Fluctuations in relative sea-level during the past 3000 yr in the Onnetoh estuary, Hokkaido, northern Japan. *J. Quat. Sci.* **17**, 607–622 (2002).
- Clague, J. J., Bobrowsky, P. T. & Hutchinson, I. A review of geological records of large tsunamis at Vancouver Island, British Columbia, and implications for hazard. *Quat. Sci. Rev.* **19**, 849–863 (2000).
- Pinegina, T. K., Bourgeois, J., Bazanova, L. L., Melekestsev, I. V. & Braitseva, O. A. A millennial-scale record of Holocene tsunamis on the Lronotskiy Bay coast, Kamchatka, Russia. *Quat. Res.* **59**, 36–47 (2003).
- Hirakawa, K., Nakamura, Y. & Echigo, T. Tokachi chiho Taiheiyō engan chiiki no kyodai tsunami [Giant tsunami along the Pacific coast of the Tokachi region]. *Gekkan Chikyu* (supplement 31), 92–98 (2000).
- Sawai, Y. Evidence for 17th-century tsunamis generated on the Kuril-Kamchatka subduction zone, Lake Tokotan, Hokkaido, Japan. *J. Asian Earth Sci.* **20**, 903–911 (2002).
- Furukawa, R., Yoshimoto, M., Yamagata, K., Wada, K. & Ui, T. Did Hokkaido Komagatake volcano erupt in 1694? — reappraisal of the eruptive ages of 17–18th centuries in Hokkaido [in Japanese with English abstract]. *Kazan* **42**, 269–276 (1997).
- Nishimura, Y., Miyaji, N., Yoshida, M., Murata, T. & Nakagawa, M. The 1843 tsunami deposits found in the peat deposit at Kiritappu marsh, eastern Hokkaido, Japan [in Japanese with English abstract]. *Daiyōki Kenkyū* **39**, 451–460 (2000).
- Chikita, K., Fukuyami, R., Sakamoto, H. & Nakamichi, K. Dynamic behaviors of “dead water” in a coastal lagoon, Lake Harutori, Kushiro, Hokkaido: Field measurements for the ice-covered period [in Japanese with English abstract]. *Geophys. Bull. Hokkaido Univ.* **60** 13–28 (1997).

20. Beck, S. L. & Ruff, L. J. Rupture process of the great 1963 Kuril Islands earthquake sequence: asperity interaction and multiple event rupture. *J. Geophys. Res.* **92**, 14123–14138 (1987).
 21. Kanamori, H. Mechanism of tsunami earthquakes. *Phys. Earth Planet. Inter.* **6**, 246–259 (1972).
 22. Okal, E. A. & Newman, A. V. Tsunami earthquakes: The quest for a regional signal. *Phys. Earth Planet. Inter.* **124**, 45–70 (2001).
 23. Tanioka, Y. & Satake, K. Fault parameters of the 1896 Sanriku tsunami earthquake estimated from tsunami numerical modeling. *Geophys. Res. Lett.* **23**, 1549–1552 (1996).
 24. Thatcher, W. Earthquake recurrence and risk assessment in circum-Pacific seismic gaps. *Nature* **341**, 432–434 (1989).
 25. Schwartz, S. Y. Noncharacteristic behavior and complex recurrence of large subduction zone earthquakes. *J. Geophys. Res.* **104**, 23111–23125 (1999).
 26. Ando, M. Source mechanisms and tectonic significance of historical earthquakes along the Nankai trough. *Japan. Tectonophysics* **27**, 119–140 (1975).
 27. Mansinha, L. & Smylie, D. E. The displacement fields of inclined faults. *Bull. Seismol. Soc. Am.* **61**, 1433–1440 (1971).
 28. Imamura, F. in *Long-wave Runup Models* (eds Yeh, H., Liu, P. & Synolakis, C.) 25–42 (World Scientific, Singapore, 1996).
 29. Satake, K. Linear and nonlinear computations of the 1992 Nicaragua earthquake tsunami. *Pure Appl. Geophys.* **144**, 455–470 (1995).
 30. Iwasaki, T. & Mano, A. Two-dimensional numerical simulation of tsunami run-ups in the Eulerian description [in Japanese]. *Proc. 26th Conf. Coastal Eng. JSCE*, 70–72 (Japan Soc. Civil Engineers, Tokyo, 1979).

Supplementary Information accompanies the paper on www.nature.com/nature.

Acknowledgements We thank K. Hirakawa, Y. Nishimura, Y. Sawai, A. Moore, H. Kelsey and E. Hemphill-Haley for guidance in the field, and F. Akiba for diatom analysis. We also thank R. Stein, J. Bourgeois, K. Shimazaki, S. Toda and H. Kelsey for comments on the manuscript. The work formed part of the US–Japan Common Agenda for earthquake and tsunami studies.

Competing interests statement The authors declare that they have no competing financial interests.

Correspondence and requests for materials should be addressed to K. Satake (kenji.satake@aist.go.jp).

The hydrodynamics of water strider locomotion

David L. Hu¹, Brian Chan² & John W. M. Bush¹

¹Department of Mathematics, and

²Department of Mechanical Engineering MIT, Cambridge, Massachusetts 02139, USA

Water striders *Gerridae* are insects of characteristic length 1 cm and weight 10 dynes that reside on the surface of ponds, rivers, and the open ocean^{1–4}. Their weight is supported by the surface tension force generated by curvature of the free surface^{5,6}, and they propel themselves by driving their central pair of hydrophobic legs in a sculling motion^{7,8}. Previous investigators have assumed that the hydrodynamic propulsion of the water strider relies on momentum transfer by surface waves^{1,9,10}. This assumption leads to Denny’s paradox¹¹: infant water striders, whose legs are too slow to generate waves, should be incapable of propelling themselves along the surface. We here resolve this paradox through reporting the results of high-speed video and particle-tracking studies. Experiments reveal that the strider transfers momentum to the underlying fluid not primarily through capillary waves, but rather through hemispherical vortices shed by its driving legs. This insight guided us in constructing a self-contained mechanical water strider whose means of propulsion is analogous to that of its natural counterpart.

Whereas substantial advances have been made in the field of biolocomotion^{9,12–16}, the hydrodynamics underlying the surface locomotion of semiaquatic insects remains poorly understood^{1,9,11,17}. There are two means of walking on water according to the relative magnitudes of the body weight Mg and the maximum

curvature force σP , where M is the body mass, g the gravitational acceleration, σ the surface tension and P the contact perimeter of the water-walker¹⁷. Water-walkers characterized by $M_c = \frac{Mg}{\sigma P} > 1$, such as the basilisk lizard, rely on the force generated by their feet slapping the surface and propelling water downward¹⁸. Creatures with $M_c < 1$, such as the water strider may reside at rest on the surface, supported by the curvature force generated by distortion of the free surface (Fig. 1). The body and legs of the water strider are covered by thousands of hairs¹ that render its legs effectively non-wetting¹⁹. During their rowing stroke, water striders drive their middle legs against the water without penetrating the surface and may achieve peak speeds of 150 cm s^{-1} . The striders may launch themselves with a vertical component, or glide along the surface.

The force balance on a stationary water strider may be understood in terms of the statics of floating, non-wetting bodies⁶. The weight of a stationary water strider is supported by some combination of the buoyancy force, F_b , and the curvature force, F_c , associated with the surface tension σ : $Mg = F_b + F_c$. F_b is deduced by integrating the hydrostatic pressure over the body area in contact with the water, while F_c is deduced by integrating the curvature pressure over this area, or equivalently the vertical component of the surface tension, $\sigma \sin \theta$, along the contact perimeter (Fig. 1b). Keller⁶ demonstrated that the ratio of F_b to F_c is equal to that of the fluid volumes displaced inside and outside the contact line. For a long thin water-strider leg, this ratio is $F_b/F_c \sim w/L_c \ll 1$, where $w \approx 40 \mu\text{m}$ is the leg radius¹, $L_c = (\sigma/\rho g)^{1/2} \approx 2 \text{ mm}$ the capillary length, and ρ the density of water. The strider’s weight is supported almost exclusively by surface tension. Figure 2 illustrates the dependence of the maximum surface tension force on body weight for 342 species of water striders. The observed dependence illustrates that as the striders increase in size, their legs become proportionately longer. It is only thus that the largest water strider (marked C in Fig. 2), *Gigantometra gigas*²⁰, whose length may exceed 20 cm, is a viable water-walker.

For the water strider to move, Newton’s third law requires that it transfer momentum to the underlying fluid. It has previously been assumed that capillary waves are the sole means by which to accomplish this momentum transfer^{1,9–11}. Denny⁹ suggested that the leg speed of the infant water strider is less than the minimum phase speed of surface waves²¹, $c_m = (4g\sigma/\rho)^{1/4} \approx 23.2 \text{ cm s}^{-1}$; consequently, the infants are incapable of generating waves and so transferring momentum to the underlying fluid. According to this physical picture, infant water striders cannot swim, an inference referred to as Denny’s paradox^{9,11}.

A series of laboratory experiments were conducted in order to elucidate the hydrodynamic propulsion mechanism of the water strider *Gerris remigis*. Water striders were collected from local freshwater ponds and maintained in aquaria. The striders reproduced every several weeks, providing the opportunity to study the first-instar nymph water striders in a laboratory setting. The striders were filmed using a high-speed video camera at 500 frames per second and the images were digitized and analysed using Midas motion analysis software. Particle tracking was performed by seeding water with either Kalliroscope or Pliolite particles of size 50–100 μm . Dye studies were performed using food colouring and thymol blue. Images of the waves and vortices generated by the strider motion were obtained from both plan and side views; their form and speed were measured directly following the stroke. The surface signature of the capillary waves was measured with a technique adopted from Schooley²².

The Reynolds number characterizing the adult leg stroke is $Re = UL_2/\nu \approx 10^3$, where $U \approx 100 \text{ cm s}^{-1}$ is the peak leg speed and $L_2 \approx 0.3 \text{ cm}$ is the length of the rowing leg’s tarsal segment (see Figs 1b and 2), which prescribes the size of the dynamic meniscus forced by the leg stroke²³. For the 0.01-s duration of the stroke, the driving legs apply a total force $F \approx 50$ dynes, the magnitude of